Direct detection submillimeter spectrometer for CCAT

Thomas Nikola,[a] Gordon J. Stacey,[a] & C. Matt Bradford[b]
[a] Cornell University, Space Sciences Bldg, Ithaca, NY 14853;
[b] Jet Propulsion Laboratory, Pasadena, CA 91109

Direct Detection Submillimeter Spectrometer for CCAT

Thomas Nikola[*a], Gordon J. Stacey[a], C. Matt Bradford[b]
[a]Cornell University, Space Sciences Bldg, Ithaca, NY, USA 14853;
[b]Jet Propulsion Laboratory, Pasadena, CA 91109,

ABSTRACT

We present a trade study for a submillimeter direct-detection spectrometer operating at the background limit for the Cornell Caltech Atacama Telescope (CCAT). In this study we compare the classical echelle spectrometer ZEUS with the waveguide grating spectrometer Z-Spec. The science driver for this instrument is spectroscopic investigation of high redshift galaxies as their far-IR fine structure line emission is redshifted into the telluric submillimeter windows. The baseline detector consists of SQUID multiplexed TES bolometers and the ideal spectrometer to detect weak lines from distant extragalactic sources is a grating with a resolution of ~10^3 and a large bandwidth, covering an entire telluric submillimeter window instantaneously. Since the density of high-z sources on the sky is ~100 within a 10′×10′ field of view and a redshift range of Δz~0.2 we also explore multi-object (~50 objects) capability, including articulated mirrors and flexible waveguide fibers.

Keywords: Submillimeter; Spectrometer; Direct-detection; Echelle; Waveguide; High-redshift

1. INTRODUCTION

The Cornell Caltech Atacama Telescope (CCAT) is envisioned as a 25 meter aperture submillimeter telescope located near the summit of Cerro Chajnantor. CCAT will have a large field of view (~20′) and high surface accuracy (~10 μm rms) mirrors. The very large, high efficiency aperture, together with the excellent site will enable large surveys utilizing the entire submillimeter and millimeter wavelength regime from 200 μm to 2.5 mm. The superb Chajnantor site permits routine spectroscopic observations in the 350 μm telluric window.

The main science topics for CCAT include: (1) the early Universe and cosmology, (2) galaxy formation and evolution, (3) cosmic microwave background and Sunyaev-Zeldovich effect, (4) disk, star, and planet formation, and (5) solar system astrophysics. The planned direct-detection spectrometer that we will discuss here will specifically address the topics of galaxy formation and evolution and the star formation history of the Universe.

About a decade ago the Cosmic Background Explorer satellite (COBE) discovered the cosmic infrared background (CIB) radiation. The CIB, which peaks at about 150 μm, is thermal emission from dust that is heated by optical/UV radiation from active galactic nuclei (AGN) and stellar photospheres. The COBE data shows that about half of the total energy emitted in the optical/UV is converted and emitted as CIB radiation, demonstrating the importance of including far-IR and submillimeter observations when investigating galaxy formation and evolution and the star formation history of the Universe. Subsequent deep observations by SCUBA, MAMBO, and Spitzer, for example, have resolved much of the CIB into optically obscured galaxies largely powered by star formation. The inclusion of the dusty infrared galaxies in studies of the star formation history of the Universe shifts the peak of star formation rate per co-moving volume to slight earlier times at redshifts between 1 and 3.

The star formation history of the Universe and galaxy formation and evolution are tightly linked, with the environment around galaxies and in galaxy clusters affecting the star formation in the galaxies externally and star formation affecting the evolution of the galaxies internally. A detailed investigation into these effects and to study the physical properties requires spectroscopic observations of the often heavily obscured galaxies. Far-IR fine structure lines (e.g. [CII], [OI], [OIII], [NII]) that are redshifted into the submillimeter wavelength regime are especially useful for this purpose, since they probe the physical conditions of atomic gas, photodissociation regions (PDRs), and ionized gas in star forming and active nuclear regions.

[*] tn46@cornell.edu

Millimeter and Submillimeter Detectors and Instrumentation for Astronomy IV
edited by William D. Duncan, Wayne S. Holland, Stafford Withington, Jonas Zmuidzinas
Proc. of SPIE Vol. 7020, 702016, (2008) · 0277-786X/08/$18 · doi: 10.1117/12.790130

It is easy to show that a background-limited, direct-detection spectrometer with resolving power matched to the expected line width is the best choice to survey the physical conditions in galaxies and star formation in galaxies at various epochs in the history of the Universe. Such a well matched instrument on CCAT will not only permit observing the most luminous galaxies, but also observing more "normal" galaxies up to z~5. This is important in order to get an unbiased view of the star formation processes and galaxy evolution in the history of the Universe. Here we will compare two designs for a direct-detection spectrometer that fit the requirements, using the submillimeter grating spectrometer ZEUS and the millimeter grating waveguide spectrometer Z-Spec as examples.

2. SCIENTIFIC JUSTIFICATION

How do galaxies form and evolve and what role plays star formation in this evolution? From observations of galaxies and star formation in the local Universe we know that interactions between galaxies and mergers of galaxies can trigger enhanced star formation. Interactions and enhanced star formation is common in groups of galaxies. Indeed, most ultraluminous infrared galaxies (ULIRGs) show disturbed morphology and often a companion or a double nucleus, indicating that they experienced a strong tidal interaction, which funneled gas toward the potential well, compressed the gas and thus triggered enhanced star formation. On the other hand, it is also known that the star formation rate in galaxies in overdense regions is reduced. This suppression of star formation can be explained by several effects. For example gas within a galaxy could be removed due to ram pressure when the galaxy moves through the intracluster medium, thus take away the reservoir needed for further star formation. A similar effect is when the hot ionized gas around galaxies gets stripped away (strangulation). This hot gas reservoir could normally fall into the galaxy when it cools and thus replenish the internal gas reservoir. When this secondary reservoir is no longer available the star formation activity in the galaxy will eventually be truncated. How do these effects affect galaxy evolution and star formation in the early Universe? The assemblage process of massive galaxies via mergers of proto-galaxies in the early Universe, and the fact that the gas fraction was higher and the galaxies were closer together, leading to higher rates of galaxy interactions, results in large star formation rates per co-moving volume. Estimates of the star formation rate per co-moving volume over the history of the Universe set the peak to redshifts of z~1-3 [10] (Fig 1). How do the physical conditions in the interstellar and intracluster medium evolve and what are the conditions at the peak in the star formation rate?

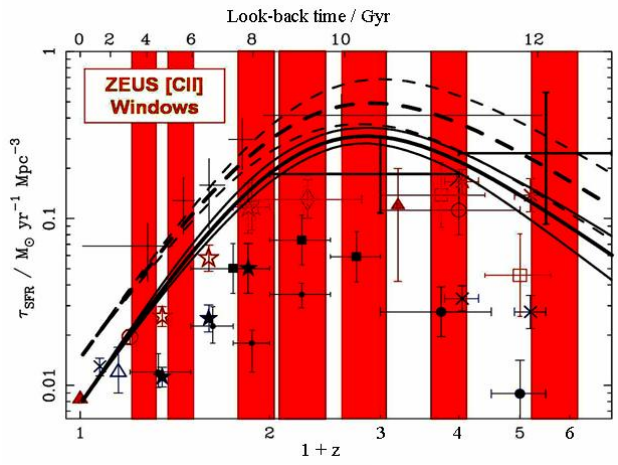

Fig. 1 Co-moving star formation history of the Universe [10]. The original Madau diagram based on optical/UV HDF observations are the filled marks. The open symbols correct this data for dust extinction. The 2 curves with error envelopes are models based on the SCUBA data. The vertical bars show the [CII] redshift ranges accessible to ZEUS on CCAT (overlap of redshifted [CII] with telluric submillimeter windows).

The detection of the cosmic infrared background radiation (CIB) by COBE and the discovery that about half of the total energy released from stars and AGNs is reprocessed and emitted in the far-IR was a major advancement in the study of galaxy evolution and the history of star formation in the Universe. Subsequent broad-band observation in the mid- and far-IR (Spitzer), submillimeter (SCUBA), and millimeter (MAMBO) resolved much of the CIB into individual objects, which turned out to be distant, optically obscured galaxies. These observations also showed that the source distribution for the different bands peaks at different redshifts (z~0.7 (15 μm), z~1.1 (24 μm), z~2.3 (850 μm) [7]) and that the luminosity functions evolve differently. The submillimeter galaxies (SMGs) detected by SCUBA are of special importance, since their source distribution peaks at the peak of the history of star formation in the Universe. The infrared luminosities of these SMGs are often quite bit larger than those of the most luminous ULIRGs in the local Universe. ULIRGs are believed to be powered by localized (<1 kpc^2), collision induced starbursts. But SMGs are most likely not just scaled up analogs of local ULIRGs. Recent observations [5],[6] suggest that SMGs undergo galaxy-wide (~10's of kpc^2) bursts of star formation, suggesting a different process

than for ULIRGs. Also SMGs tend to be very massive galaxies, suggesting that they are galaxies in the process of becoming giant elliptical galaxies that are found in the potential well of galaxy clusters.

Investigating the history of the star formation rate and galaxy formation and evolution requires spectroscopic observations. Only spectroscopy can provide the detailed information necessary for a deeper understanding. Especially useful are far-IR fine structure lines that are redshifted into the submillimeter wavelength regime. Figure 1 shows the diagram of the history of the star formation rate per co-moving volume. Overplotted are vertical bands that indicate the redshifts for which the [CII] 158 μm fine structure line will fall within a telluric window in the submillimeter regime. It is obvious that the [CII] line can be observed over more than 50% of the redshift range. The [CII] fine structure is expected to be the brightest far-IR line in starburst galaxies. Apart from the [CII] line the rest-frame far-IR regime includes the [NII] 122 and 205 μm, the [NIII] 57 μm, and the [OIII] 52 and 88 μm fine structure lines. These lines probe the hardness of the UV field as well as the density of HII regions. The ratio of the [NIII] and [OIII] is also a good indicator for the age of the interstellar medium. The rest-frame far-IR also includes the important [OI] 63 and 146 μm fine structure lines. In dense, warm photodissociation regions (PDRs) the [OI] 63 μm line can be stronger than the [CII] line.

The [CII] 158 μm fine structure line is an excellent tracer for star formation activity and will be the main tracer to probe the physical conditions in the star forming regions. It is the primary cooling line for PDRs within galaxies, and one of the brightest single emission lines on galactic scales. In a PDR scenario dust is heated by the energy emitted from massive stars and cools via infrared continuum emission. The gas is heated mainly via the photoelectric effect from dust grains, where far-UV photons are absorbed by dust grains and subsequently eject an electron with excess kinetic energy. Gas cooling is due to the far-IR fine structure lines and rotational transitions of CO. For the densities and temperatures in PDRs in active star forming regions the [CII] line to far-IR continuum luminosity ratio is inversely proportional to the strength of the far-UV radiation field, parameterized in units of the local far-UV radiation field G_o. This is due to the reduced efficiency of the photoelectric effect of charged grains and the increased importance of cooling from the 63 μm [OI] line. Therefore, the [CII] line to far-IR continuum radio determines the strength of the far-UV field G. By comparing the derived G with the observed far-IR continuum one obtains the beam filling factor and thus the extent of the star forming region.

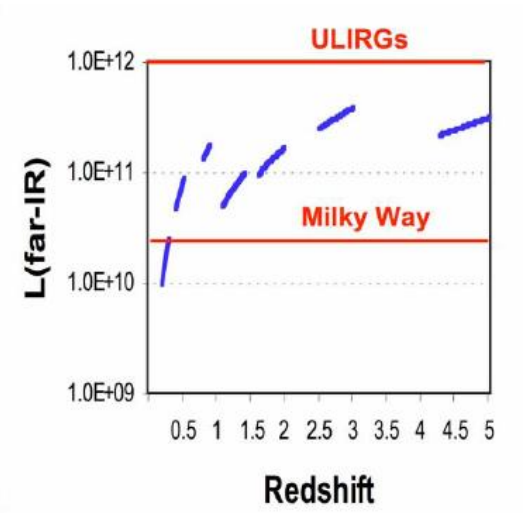

Fig. 2 Required minimum far-IR luminosity for detecting the [CII] line in galaxies with a Milky Way type $L_{[CII]}/L_{far\text{-}IR}$ ratio (5σ, 4 h).

The [CII] line to far-IR continuum ratio is largest for "normal" star forming galaxies (~0.1 to 1%), with modest far-UV fields like those observed in the Milky Way, relatively small for ULIRGs (~0.06%). The relative weakness of the line from ULIRGs likely reflects the very intense radiation fields in the compact ULIRG starbursts. Since the [CII] line to far-IR continuum ratio grows for lower luminous sources the [CII] line from galaxies that are only a few times more luminous than our own can be observed from the same redshifts as ULIRGs. This is shown in figure 2. The thick short lines in figure 2 represent the minimum far-IR luminosity a galaxy with a Milky Way type $L_{[CII]}/L_{far\text{-}IR}$ ratio needs in order to detect the [CII] line with CCAT (5σ, 4 hours). It shows that the [CII] line can be detected in galaxies with $L_{far\text{-}IR}>3\times10^{11}$ $L_{\odot}$ and a Milky Way ratio of $L_{[CII]}/L_{far\text{-}IR}$~0.3% at redshifts in excess of z=5. For ULIRGs the [CII] line will readily be detectable for galaxies with $L_{far\text{-}IR}>1.5\times10^{12}$ $L_{\odot}$.

It is also instructive to compare the signal-to-noise ratio of the [CII] observation with continuum observations. For a Milky Way luminosity ratio and an optimally resolved line the line to continuum ratio is ~5:1. An optimized spectrometer with a spectral resolution of R=1000 is ~10 times less sensitive than an optimized photometer with R~10. Therefore the line is detected at only 2 times worse signal-to-noise ratio than the continuum in the same integration time.

As shown above, with a direct detection spectrometer on CCAT it will be possible to observe the [CII] line from not only most luminous sources, but also from less luminous infrared galaxies with Milky Way type star formation activity. This is very important when studying the star formation activity in the early universe and galaxy evolution in clusters,

since it permits comparing different star formation modes from different types of galaxies and not just from the most luminous ones.

3. CORNELL CALTECH ATACAMA TELESCOPE (CCAT)

The Cornell Caltech Atacama Telescope (CCAT) is planned to be built near the summit of Cerro Chajnantor (5600 m) and to be completed sometime near 2014. Placing CCAT at this site, which is next to the ALMA site on the Chajnantor plateau (5000 m), but 600 meters higher provides significant improvements in the atmospheric transmission in the submillimeter telluric windows compared to the transmission at the plateau. For example for a quarter of the time the zenith opacity at 350 μm is below 1.1 at the CCAT site while it is only below 1.4 at the Chajnantor plateau (CBI site). In other words the zenith opacity at 350 μm is below 1.2 for about 30% of the time at the CCAT site compared to 15% of the time at the CBI site [9]. Observations at 350 μm will thus become the routine. The CCAT site also has excellent transmission at the 200 μm telluric window allowing significant fraction of time for observations in this band.

CCAT will have an aperture with a diameter of 25 meter and the surface accuracy of the telescope will be ~10 μm, ensuring good performance at wavelengths as short as the 200 μm. The field of view will be about 20 arcmin. At 350 μm the diffraction limited beam size is about 3.5 arcsec and at 450 μm it is 4.5 arcsec. Thus a 10′×10′ field on the sky can be covered by about 30,000 diffraction limited beams at 350 μm or 18,000 diffraction limited beams at 450 μm.

More information about CCAT can be found on the website www.submm.org

4. MULTI-OBJECT SPECTROSCOPY

To take full advantage of the large field of view provided by CCAT it is best to carry out spectroscopy of as large a field as possible. For a detector with a given number of pixels a Fabry-Perot interferometer would cover the largest field of view for doing spectroscopy. However, a Fabry-Perot interferometer needs to spectrally scan to provide detection of both the line and adjacent continuum, resulting in a large penalty in on-line integration times for line detection. On the other hand an integral field unit or image slicing design provides an instantaneous spectrum, but necessarily a smaller field of view. Given that the distant galaxies will be point sources that are distributed over the telescope field of view the integral field unit with its limited and contiguous field is not the best solution. Furthermore, sources will be sparsely distributed with the field of view so that an imaging Fabry-Perot is also not the best choice. The preferred solution is a multi-object spectral multiplexing grating spectrometer with multiple movable feeds that can pick out sources widely and randomly distributed with the field of view of the telescope.

4.1 Number of Beams

To determine the number of beams for a multi-object spectrometer we estimate the expected source density for [CII] spectroscopy with CCAT using galaxy counts at 850 μm. The flux density for a star forming ULIRG ($L_{far\text{-}IR}>10^{12}L_{\odot}$; Arp220 like) in the 850 μm SCUBA band is about 1 mJy over the entire redshift range of z~1-10 [10]. This is due to the negative K-correction. A LIRG ($10^{11}L_{\odot}<L_{far\text{-}IR}<10^{12}L_{\odot}$) would be ten times weaker. From an estimate of the cumulated source density as a function of flux density for 850 μm we then obtain a galaxy number density of about 70,000 galaxies per square degrees for galaxies with luminosities greater than 10^{11} L_{sun} (LIRG+) [1]. This galaxy number density is basically over the entire redshift range. However, the [CII] 158 μm line is only accessible within finite redshift ranges in the telluric windows (see Figure 1). The redshift range of z=1-1.2 covers about half of the 350 μm telluric window and the redshift range of z=1.8-2 covers about half of the 450 μm telluric window. Using models of the redshift distribution for 850 μm galaxy counts [1] we estimate that about 4.8% of the 850 μm galaxies are within the redshift range of z=1-1.2 and about 5.8% of the 850 μm galaxies are within the redshift range of z=1.8-2. Assuming a spectral resolution of R~1000 this then results in 3400 LIRG+ galaxies per square degrees in the redshift range of z=1-1.2 or about 95 LIRG+ galaxies in a 10′×10′ field. Similarly we obtain about 114 LIRG+ galaxies within a 10′×10′ field of view in the redshift range of z=1.8-2. On the other hand an observation of the galaxy protocluster J2142-4423 with LABoCa revealed about 22 sources within a 10 arcmin field of view [2]. A multi-object pick-up arrangement with ~50 units would therefore be a good choice. The spectrometers then also need to be designed to accept 50 beams.

4.2 Dielectic Fibers

One possibility for the multi-object pick-up unit is to use dielectric fibers. A fiber fed multi-object design is compact and light weight and fiber fed assemblies have been used in the optical and near- and mid-IR. They can in principle be

attached to masks mounted at the telescope focal plane or held in place by mechanical arms. However, finding a proper material that can be used for fibers in the submillimeter wavelength regime is difficult. The fibers need to have good flexibility, good transmission, and low bending losses. In addition the fibers need to have very low emissivity, so that they don't contribute to the background noise. The length of the fibers need to be in the order of one meter. Glenn et al. at UC Boulder is currently investigating the properties of hollow polycarbonate tubing for this purpose with some success.

4.3 Mirror Assembly

Another possibility for a multi-object pick-up design is using a collection of mirror that are mounted on mechanical arms and that can be freely positioned in the focal plane of the telescope. Mirrors have very small losses and low emissivity. However, the detailed mechanical design can be challenging. Mirrors are much heavier than fibers and the weight and therefore the stability could become a problem. In addition it should be possible to arrange the mirrors in a very compact configuration for observations of crowded fields, or extended emission.

4.4 Field Rotator

A multi-object spectrometer will require a field rotator to compensate for the rotation of the field of view during the observation. We envision a set of fore-optics with a so-called K-mirror to compensate for the rotation of the field. K-mirrors are widely used at various observatories and is probably the best solution for CCAT as well.

5. SPECTROMETER

We have narrowed down the selection for a submillimeter grating spectrometer for CCAT to two design concepts. Each of them is currently used in a state of the art spectrometers, one in the submillimeter wavelength regime and the other in the millimeter wavelength regime. In this section we compare both design concepts using these existing spectrometers as examples.

5.1 Classical Echelle Spectrometer (ZEUS Type)

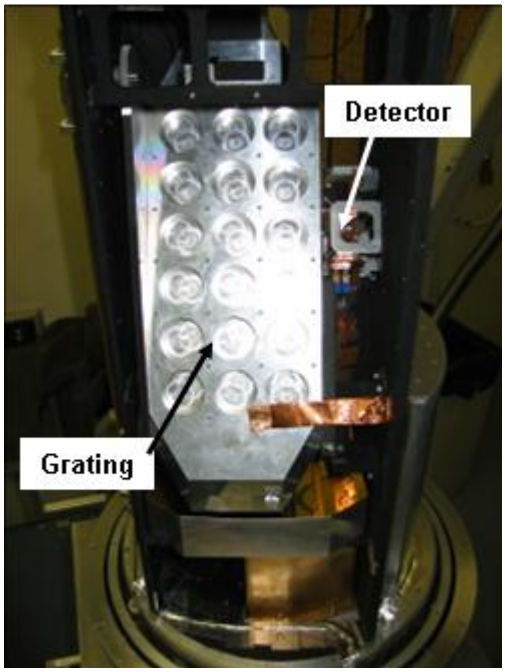

Fig. 3 ZEUS

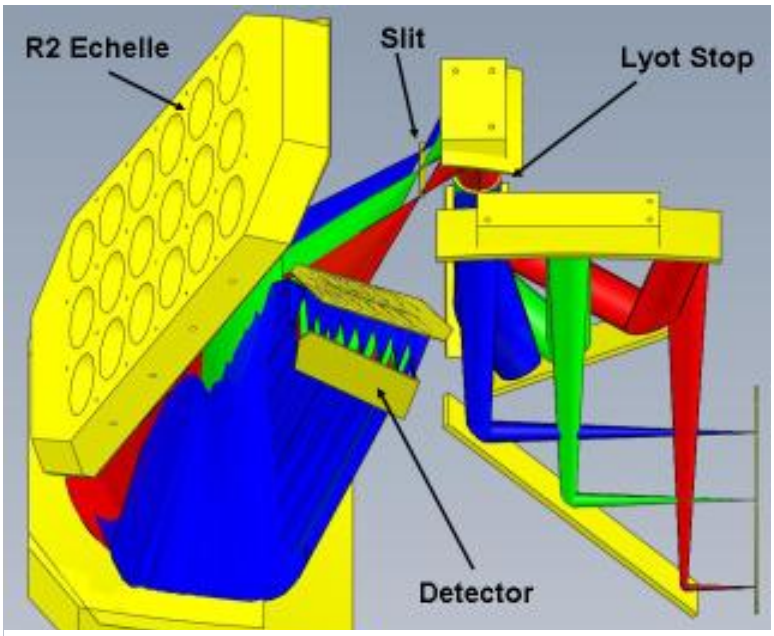

Fig. 4 Optical Layout of ZEUS 2. Optical path of 3 spatial beams through the mirror assembly of ZEUS 2.

At Cornell University we have built the submillimeter echelle spectrometer, ZEUS [11] (Fig. 3). It has a spectral resolution of about 1200 and is currently equipped with a 1×32 pixel thermistor sensed bolometer detector array. The 32 pixels are lined up along the dispersion direction. ZEUS has a R2 echelle to obtain high efficiency over a wide

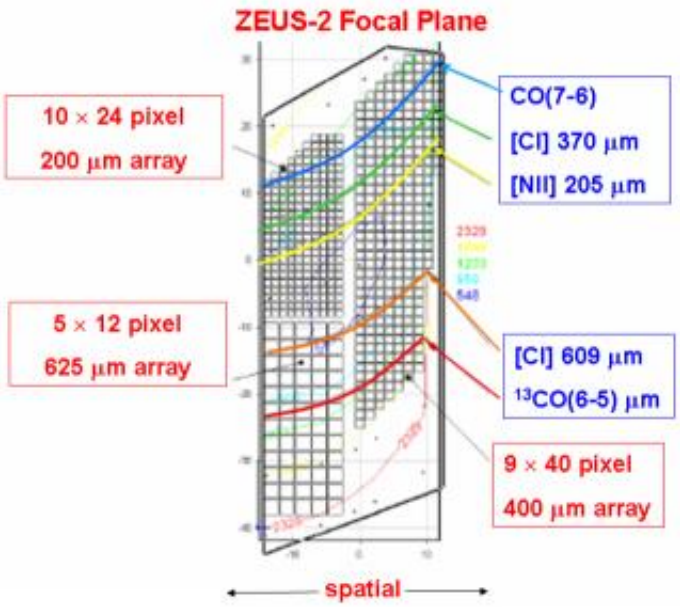

Fig. 5 Pixel layout of focal plane array of ZEUS 2. The focal plane consists of 3 distinct bolometer arrays tuned to work at 200 μm, 400 μm, and 625 μm. The underlying contour lines with numerical label denote the geometric spot size distribution. The thick curved lines overlayed on the pixels show the location of 5 specific emission lines that can be observed simultaneously.

wavelength range and it is designed so that the 5th, 4th, and 3rd order coincide with the 360 μm, 450 μm, and 600 μm telluric windows. The length of the echelle is only 35cm. We are currently upgrading ZEUS with a new detector array and a new cooling system. The new ZEUS 2 will be a completely separate instrument, but will use the original echelle grating from ZEUS. Figure 4 shows the optical path of three spatial beams through ZEUS 2. The beams enter the instrument from the right hand side. Then the beams are collimated and pass through a cold pupil (Lyot stop) before they are re-imaged at the entrance slit. After the slit the beams are collimated again. The grating is at the pupil position in the collimated beam. The dispersed beams are then finally re-imaged onto the detector array. It is a classical optical design for an echelle spectrograph with the grating operating in Littrow mode and including a cold pupil (Lyot stop) and a cold entrance slit. The grating can be tilted in order to select the desired wavelength coverage. The focal plane in ZEUS 2 will be populated with 9×40 pixel array tuned for work at 400 μm, a 10×24 pixel array tuned for work at 200 μm, and a 5×12 pixel array tuned for work at 625 μm (Fig. 5). They are arranged so that they accommodate variations in the geometric spot size over the focal plane and so that the CO (7-6) and ^{13}CO (6-5) rotational transitions, the [CI] 371 μm and 609 μm fine structure line and the [NII] 205 μm fine structure line can be observed simultaneously. Thus, although the individual telluric windows are not fully spectrally covered, by observing selected wavelength ranges in several telluric bands simultaneously we maximize the line observing efficiency.

A similar design can be envisioned for a multi-object spectrometer for CCAT. Since the echelle will be at a pupil position the size of the grating will not change with the number of beams. To cover a wider wavelength range with high grating efficiency, the echelle can be operated at lower order. To obtain a resolution of R~1500 at 350 μm with an R1 echelle the projected beam size is still only 37 cm and the physical size of the echelle is still a modest 52 cm. In this design the echelle can be tilted to cover entire telluric windows. The ability to tilt the grating has the additional advantage to direct the dispersed wavelength to specific pixels to maximize the efficiency.

5.2 Waveguide Spectrometer (Z-Spec Type)

A novel design for a grating spectrometer is employing a curved grating based on a Rowland circle grating design that is enclosed in a waveguide [3][8] (Fig. 6). The waveguide consists of two plane plates parallel to the meridional plane of the Rowland circle design (Fig. 7). The spacing between the parallel plates is matched to the first transversal electrical mode (TE_1) of the main wavelength of interest. A single-mode waveguide couples the incident wave into the waveguide grating arrangement and similarly waveguides couple the dispersed wavelengths at the output to individual detector pixels. The exact positions of the facets along a smooth curve are individually calculated, as are the positions of the output waveguides for the specific wavelength. This design was successfully implemented in Z-Spec [4], a spectrometer for the 1-1.6 mm wavelength regime that currently operates at the CSO. Z-Spec operates at first order providing spectral resolutions between 250 and 400 and uses 160 detector pixels covering the entire 1 to 1.6 mm range instantaneously.

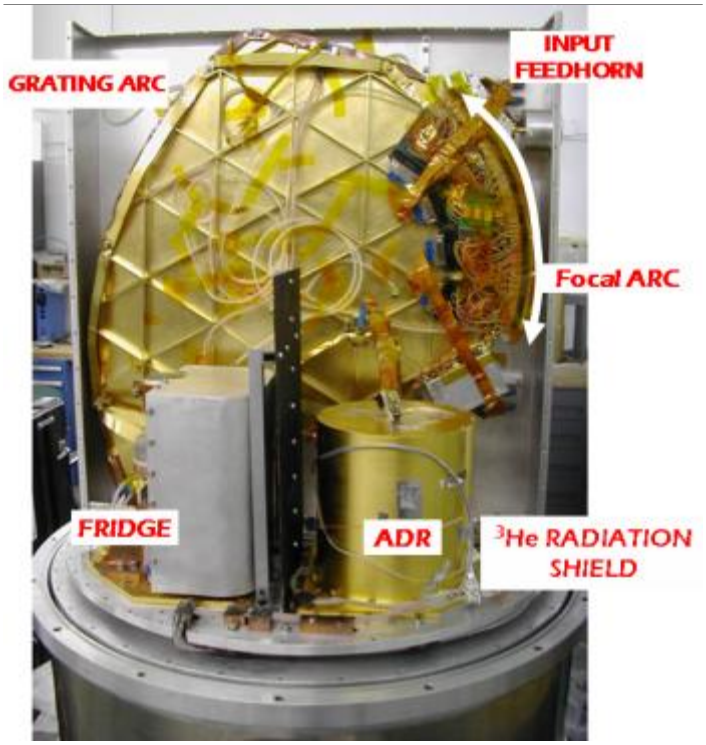

Fig. 6 Waveguide module in the Z-Spec cryostat.

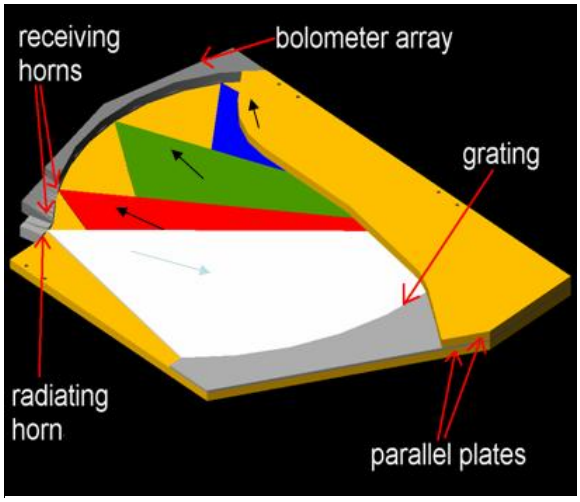

Fig. 7 Schematic of the waveguide grating module concept. Part of the top plate of the waveguide is cut away. The "white light" enters the waveguide through the radiating horn on the left. The curved grating on the right focuses the dispersed light onto the receiving horns, which feed the radiation to the bolometers [3].

A demonstration model for the short submillimeter regime of 160-300 μm is currently being fabricated and tested. This demonstration model has a spectral resolution of 1000 to 1600 and employs 500 detector pixels to cover the entire wavelength regime simultaneously [4]. By stacking several of these curved waveguide grating assemblies it will be possible to observe a one dimensional field of view or several individual beams. However, the thickness of the waveguide plates could make this approach prohibitively large. A new design that uses a thick silicon wafer as the transmitting medium and with the surfaces metallized is currently investigated for the far-IR regime [4]. Such a waveguide design can be closely stacked with the limit now set by the size of the waveguide for the incident waves. Due to the high refractive index of silicon this new design also becomes much smaller.

This design of stacked, curved waveguide grating using individual thick silicon wafers has several advantages. It does not require additional fore-optics other than bandpass and cut-on filters (mounted to e.g. radiation shields), it is compact, has no moving parts, and the estimated efficiency (in one polarization) is very good. Calculations show that the blaze and ohmic propagation losses should be less than 10%.

5.3 Comparison between ZEUS Type and Z-Spec Type Spectrometer

For a single beam the Rowland circle grating design and the waveguide approach of Z-Spec is more compact than a ZEUS type spectrometer. However, when increasing the number of beams the compactness advantage of a Z-Spec type instrument becomes much less pronounced. This is due to the fact that several waveguide modules need to be stacked together, while the grating size of a ZEUS type instrument stays constant. On the other hand, a silicon waveguide design for a Z-Spec type instrument would reduce the size significantly so that even when stacking several of these waveguides together it would still be more compact than a classical ZEUS type design.

Having no moving parts reduces the chance of component failure. However, this is not a real problem for ground based observatories where instruments can be easily repaired. Having moving parts could actually be an advantage, since this adds flexibility. For example, it allows one to select a specific (unusually sensitive) pixel to be linked to a specific wavelength, thus maximizing line detection sensitivity. Furthermore, one can move a marginally detected line to another pixel to confirm the line detection.

The ZEUS type design propagates both polarizations, while the Z-Spec type design only allows for one polarization. But typically the grating efficiency for polarization parallel to the grating grooves is smaller than that for polarizations perpendicular to the grating grooves so that the advantage in throughput of a ZEUS-like design is only ~20%.

The 1st order Rowland circle grating design of Z-Spec provides a huge bandwidth with high efficiency in a single polarization. However, a ZEUS type spectrometer could also be designed for low order operation and thus increased efficiency over a large bandwidth. In principle a single Z-Spec type waveguide module could be designed so that it covers both the 350 and the 450 μm telluric windows.

The compact design of a Z-Spec type waveguide with the detectors attached to the waveguide requires the entire waveguide to be cooled down to the operation temperature of the detector. This in principle reduces the background radiation. In a mirror design, the mirrors can be at 2 K, the residual background is then filtered by bandpass filters at milli-K temperatures near the focal plane. Having to cool down the entire waveguide could be a disadvantage, since it requires more cooling power than a ZEUS type instrument where only the detector package needs to be cooled down to the detector operation temperature.

One big advantage of the waveguide design is the elimination of stray radiation. In submillimeter spectroscopy it is essential to reduce the background and stray radiation as much as possible in order for the spectrometer to be background limited. Although it can be done, as demonstrated in ZEUS, suppression of stray light is more of a challenge in the open structure ZEUS-type design than the closed waveguide Z-Spec design.

In a next design step we will test merging the Z-Spec with the ZEUS design and model a 2-dimensional Rowland circle grating that combines the advantages of both instruments. The goal is a spectrometer design that provides maximum observing efficiency.

6. DETECTOR

A direct-detection system is in principle more sensitive than a heterodyne system, if the direct-detection system is background noise limited and both systems have the same throughput-quantum efficiency product. This is due to the quantum noise limit of heterodyne systems. In addition, the envisioned spectrometer will have a large instantaneous spectral coverage. The goal is to cover an entire telluric band instantaneously, which is about 140 GHz at 830 GHz.

The current state of the art direct detection bolometer array consists of absorbers with appropriately positioned back short, transition edge sensors (TES) to measure the temperature, and SQUID multiplexed readout electronics (e.g. SCUBA 2). Depending on the final design of the CCAT short submillimeter spectrometer we envision either a waveguide fed bolometer array (for a Z-Spec type spectrometer) or a focal plane bolometer array (for a ZEUS type spectrometer). For the waveguide design the detector array needs to be subdivided into smaller modules that can be mounted to the waveguide. The number of pixel in the dispersion direction will be in the order of 250. For a spectral resolution of R~1500 and pixels matched to a resolution element at 350 μm, 250 pixel will cover the entire 350 μm telluric window. Since we desire 50 spatial beams on the sky we then require a 50×250 pixel array.

6.1 Sensitivity

The photon noise equivalent power for a background-limited spectrometer with warm optical elements at temperature T, emissivity ε, and cold optical elements of transmission τ (emissivity 0) and detector quantum efficiency η, is given by:

$$NEP_{ph} = h\nu\left(\frac{2A\Omega}{\lambda^2}\Delta\nu\varepsilon\eta\tau\,\tilde{n}\left(1+\varepsilon\eta\tau\,\tilde{n}\right)\cdot 2\right)^{1/2} \qquad \text{Watts/Hz}^{1/2},$$

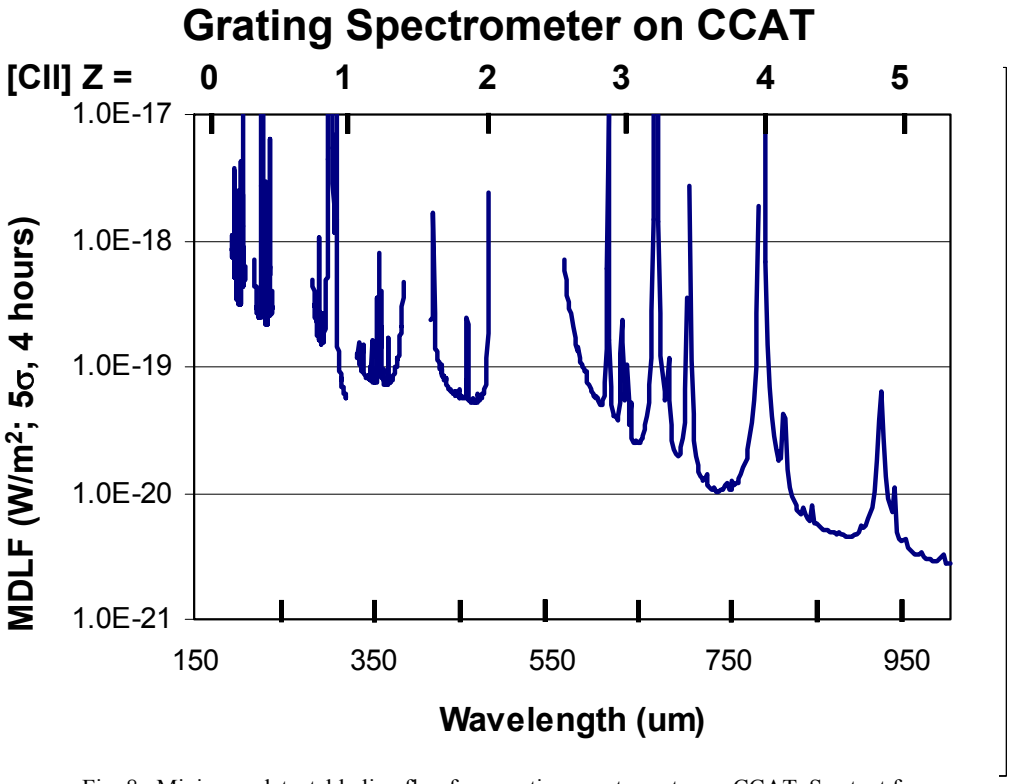

Fig. 8 Minimum detectable line flux for a grating spectrometer on CCAT. See text for details.

where h is Planck's constant, ν is the frequency, $\Delta\nu = \nu/R$ is the detection bandwidth, $A\Omega/\lambda^2$ is the number of photon modes (~1), $\tilde{n} = 1/(\exp(h\nu/kT)-1)$ is the mode occupation number, and the factors of 2 arise from detecting both polarizations (Z-Spec will only see one polarization), and expressing the NEP in $Hz^{-1/2}$. Figure 8 shows an estimate of the minimum detectable line flux for a background limited grating spectrometer. The resolution was matched to the slit sizes, but is typically R~1000. The telescope efficiencies are calculated from the Ruze formula assuming a surface accuracy of 9 μm. The sensitivity calculation assumes a precipitable water vapor (PWV) of 0.6 at the 350 μm and longer wavelength telluric windows and a PWV 0.2 for the short submillimeter telluric bands at 200 and 230 μm.

Acknowledgement This research is supported by NSF grants AST 0705256, and AST 0722220

REFERENCES

[1] Baugh, C.M., Lacey, C.G., Frenk, C.S., Granato, G.L., Silva, L., Bressan, A., Benson., A.J., and Cole, S., MNRAS, 356, 1191 (2005)
[2] Beelen, A., Omont, A., Bavouzet, N., et al., A&A, submitted (2008)
[3] Bradford, C.M., Naylor, B.J., Zmuidzinas, J., et al., Proc. SPIE, 4850, 1137 (2003)
[4] Bradford, C.M., Ade, P.A.R., Aguirre, J.E., et al., Proc. SPIE, 5498, 257 (2004)
[5] Chapman, S.C., Smail, I., Windhorst, R., Muxlow, T., and Ivison, R.J., ApJ, 611, 732 (2004)
[6] Hailey-Dunsheath, S. et al. in preparation (2008)
[7] Lagache, G., Puget, J.-L., Dole, H., ARA&A, 43, 727 (2005)
[8] Naylor, B., Ade, P.A.R., Bock, J.J., et al., Proc. SPIE, 4855, 239 (2003)

[9] Radford, S.J.E., Giovanelli, R., Sebring, T.A.., and Zmuidzinas, J., 18th International Symposium on Space Terahertz Technology, arXiv:0704.3031R (2007)
[10] Smail, I., Ivison, R.J., Blain, A.W., and Kneib, J.-P., MNRAS, 331, 495 (2002)
[11] Stacey, G.J., Hailey-Dunsheath, S., Nikola, T., Parshley, S.C., Benford, D.J., Moseley, S.H. Jr., Staguhn, J.G., Shafer, R.A., Proc. SPIE, 5498, 232 (2004)